JOURNAL OF APPLIED PHYSICS **113**, 103704 (2013)

The formation of Ti–O tetrahedra and band gap reduction in SiO_2 via pulsed ion implantation

R. J. Green,[1,a)] D. A. Zatsepin,[2,3] A. Hunt,[1] E. Z. Kurmaev,[2] N. V. Gavrilov,[4] and A. Moewes[1]
[1]*Department of Physics and Engineering Physics, University of Saskatchewan, Saskatoon, Saskatchewan S7N 5E2, Canada*
[2]*Institute of Metal Physics, Russian Academy of Sciences-Ural Division, 18 Kovalevskoi Str., 620990 Yekaterinburg, Russia*
[3]*Ural Federal University, 19 Mira Str., 620002 Yekaterinburg, Russia*
[4]*Institute of Electrophysics, Russian Academy of Sciences-Ural Division, 620016 Yekaterinburg, Russia*

(Received 21 January 2013; accepted 27 February 2013; published online 13 March 2013)

Titanium ions are implanted into amorphous SiO_2 at two different fluences using pulsed ion implantation, and the resulting samples are annealed. Bulk sensitive soft X-ray absorption spectroscopy of the Ti $L_{2,3}$ edge reveal strikingly different spectra for the two fluences. Spectral simulations using multiplet crystal field theory show clearly that for low fluence the Ti ions have a local octahedral coordination, while at higher fluence the formation of Ti^{4+}–O tetrahedra dominates. Using O *K*-edge X-ray absorption and emission, the effect of the Ti states on the valence and conduction bands of the host SiO_2 is revealed. With the introduction of Ti tetrahedra, the band gap reduces from about 8 eV to just over 4 eV, due entirely to the Ti 3*d* conduction band states. These results demonstrate the possibility to obtain Ti–O tetrahedra in silica by Ti ion implantation and a suitable thermal treatment, clarify the mechanism of band gap reduction with Ti doping in SiO_2, and demonstrate the sensitivity of *L*-edge X-ray absorption with a multiplet crystal field theory analysis to the Ti coordination of novel materials. © *2013 American Institute of Physics*. [http://dx.doi.org/10.1063/1.4795262]

I. INTRODUCTION

In recent years, the incorporation of 3*d* transition metals into semiconductors like ZnO and dielectrics like SiO_2 has been the topic of a vast number studies. Such materials show promise for a variety of technological applications based on the properties induced by the metal atoms. In some cases, the homogenous doping of transition metals into semiconductors leads to bulk ferromagnetic behavior, rendering the resulting material a dilute magnetic semiconductor[1] useful for spintronics[2] applications. Alternatively, using ion beam synthesis, the formation of metallic or metal-oxide embedded nanoparticles can be achieved.[3,4] Dielectrics with embedded nanoparticles exhibit many useful properties such as nonlinear optical behavior, superparamagnetism, intense photoluminescence, and altered band structures.[5,6]

The incorporation of Ti ions into SiO_2 (SiO_2:Ti) is an exciting topic because of the electronic properties of the constituents. The combination of the abundant Ti 3*d* conduction band states (due to the formally empty 3*d* shell of Ti^{4+}) and the very wide band gap of SiO_2 implies a situation for strong electronic structure modification upon doping. Several synthesis techniques have been employed to study SiO_2:Ti in the past, including flame hydrolysis,[7] the sol-gel method,[8–11] chemical reduction,[12] and ion implantation.[13–17] For certain Ti concentrations using flame hydrolysis or sol-gel, tetrahedral Ti^{4+} coordination has been found.[7–9,11] However, using the ion implantation technique, only indirect evidence using UV absorption has been found for T_d coordination[14] so far. Other ion implantation studies revealed metallic Ti (Ref. 15) and Ti-composite nanoclusters.[13,16,17]

The strong electronic structure modifications expected for SiO_2:Ti as alluded to above have also been only indirectly studied. A reduced band gap of 4 eV was found using optical absorption[7] (compared to the pure SiO_2 gap of 8–9 eV). However, the individual valence and conduction bands have yet to be probed in the same experiment to show the mechanism behind this gap reduction. A full understanding of this process could yield a method to tailor the band gap through Ti doping.

In the current work we study the implantation of Ti ions into amorphous, bulk SiO_2 using periodically pulsed ion implantation followed by thermal annealing. A combination of soft X-ray absorption (XAS) and X-ray emission spectroscopy (XES) is used to directly study the coordination of the Ti ions and the effects of implantation on the bulk electronic structure. Using Ti *L*-edge XAS and multiplet crystal field theory, we show that low fluences lead to octahedrally coordinated Ti while higher fluence promotes the formation of Ti–O tetrahedra. Oxygen *K*-edge XAS and XES reveal the hybridization of the Ti 3*d* and O 2*p* states for the Ti–O tetrahedra and show that the band gap narrowing is almost entirely a consequence of the Ti 3*d* states lowering the conduction band minimum. Our results demonstrate the utility of $L_{2,3}$ XAS for characterizing the Ti coordination in novel materials, demonstrate necessary parameters for producing Ti–O tetrahedra using ion implantation, and reveal the mechanism behind the band gap reduction in SiO_2:Ti.

a)Electronic mail: robert.green@usask.ca.

II. MATERIALS AND METHODS

The amorphous SiO_2 (a-SiO_2) samples used as targets for this study were 99.9% purity, plane-parallel glass plates measuring $1 \times 1\,cm^2$ with surfaces of optical quality and thicknesses of ~0.7 mm. Samples were irradiated with Ti^+ ions using a pulsed source with an ion beam current density of $\sim 2-7\,mA/cm^2$, implantation energy of 30 keV, and a pulse duration of 400 μs. Ion fluences of $1 \times 10^{15}\,cm^{-2}$ and $5 \times 10^{16}\,cm^{-2}$ were used for two separate samples. During implantation the sample temperature was kept at 250 °C. After implantation the samples were annealed in air at 1000 °C for 1 h. A high-purity a-SiO_2 sample was also left unirradiated for use as a reference material.

An additional reference sample consisting of a TiO_2:SiO_2 mixture with 8% TiO_2 by weight was synthesized via melting 99.9% purity TiO_2 and SiO_2 in a corundum crucible. This stoichiometry corresponds atomic percentages of 2.0% Ti, 31.3% Si, and 66.7% O, or $(Si_{0.94}Ti_{0.06})O_2$. The sample was melted under normal atmosphere at 2000 °C for 3 h and then slowly cooled. All samples under study and references were prepared in the Ural Federal University (Yekaterinburg, Russia) using methods developed there.[18]

The depth dependence of the Ti ion concentration was calculated using the SRIM program.[19] Simulations were performed using the same materials and implantation parameters implemented in experiment. The implantation of a total number of 10^5 ions was simulated in order to obtain an adequately converged profile. Note that SRIM does not consider dynamic changes in the host material during the implantation process, so there is no fluence dependence in the profile shape.

Soft XES were measured using Beamline 8.01 of the Advanced Light Source (ALS) at Lawrence Berkeley National Laboratory.[20] The beamline uses a Rowland circle type diffraction grating spectrometer with a 90° scattering angle, and the incident radiation is plane-polarized within the horizontal scattering plane. Soft XAS were measured using the spherical grating monochromator (SGM) beamline of the Canadian Light Source (CLS) at the University of Saskatchewan.[21] To ensure the entire implantation region was probed, spectra were collected using the bulk sensitive total fluorescence yield detection scheme, again with horizontal plane-polarized incident radiation. Note that for the $L_{2,3}$ edges of transition metal systems often the fluorescence yield is not a true measure of the XAS since the $3d \rightarrow 2p$ decay strengths can vary strongly for different XAS final states.[22] However, for Ti^{4+} the $3s$ fluorescence channel is about as equally strong as the $3d$, significantly suppressing the deviations from XAS.

To analyze the Ti $L_{2,3}$ XAS spectra, multiplet crystal field theory (MCFT) simulations were performed.[23] The simulations include full multiplet effects, as well as crystal field perturbations from neighbouring atoms. The calculated spectra were convolved with Lorentzian and Gaussian lineshapes to account for lifetime and experimental broadening, respectively.

III. RESULTS

Figure 1 shows the simulated concentration profile of Ti implanted in SiO_2 using the parameters implemented in our experiment. From the simulation we find a projected range of $R_p = 31.8$ nm with a standard deviation (or straggle) of $\sigma_{R_p} = 11.8$ nm. Within the SRIM approach, there is no dependence of the profile shape on fluence, but different fluences will obviously lead to different concentrations. Thus, on the left axis of Figure 1 we give the Ti concentration considering an implantation fluence of 5×10^{16} cm^{-2} while the right axis gives the concentration simulated for a fluence of 1×10^{15} cm^{-2}. The horizontal lines of the figure indicate the maximum Ti concentration (η_{max}, determined from the peak of a Gaussian lineshape fit to the profile) and the average Ti concentration (η_{ave}). For the higher fluence we find $\eta_{max} = 19.5$ at. % and $\eta_{ave} = 6.9$ at. % while for the lower fluence we find values of 0.39% and 0.14%, respectively. Thus the two fluences give average concentrations above and below the Ti concentration of the SiO_2:TiO_2 reference sample (2.0 at. %, as described earlier).

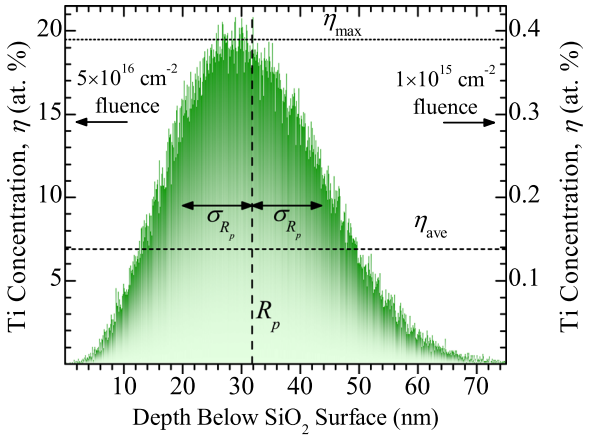

FIG. 1. Ti concentration as a function of depth for the implanted samples. The left axis shows concentration for the 5×10^{16} cm^{-2} fluence used in experiment, while the right axis is scaled for the 1×10^{15} cm^{-2} fluence. Lines are shown to indicate the projected range (R_p), the standard deviation of the projected range (σ_{R_p}), and the average and maximum concentrations (η_{ave} and η_{max}).

Figure 2 shows the experimental Ti $L_{2,3}$ XAS spectra for the implanted and reference samples. These spectra arise from the resonant excitation of Ti $2p$ electrons into bands of largely $3d$ character and are consequently very sensitive to the Ti oxidation state and coordination geometry. Immediately evident from Figure 2 is that there are striking differences between the spectra for the implanted samples prepared with different fluences. The spectrum for the higher fluence (5×10^{16} cm^{-2}) sample is very similar to that of the SiO_2:TiO_2 reference sample while the lower fluence (1×10^{15} cm^{-2}) sample exhibits different peak intensities and splittings. A spectrum recorded from rutile TiO_2 is shown in Figure 2 for reference. The spectrum looks very different from the other spectra, but as we shall show the characteristic lineshape from each sample is due to the local bonding symmetry. The different lineshapes are not due to a changing oxidation state; all samples are 4+. A look at the vastly different multiplet structure of a d^1 Ti^{3+} ion confirms this.[24]

Transition metal $L_{2,3}$ XAS spectra of oxides and related materials are generally well understood[23,25] and are well described by MCFT. For the Ti^{4+} cases shown here, the spectra can be roughly divided into two slightly overlapping

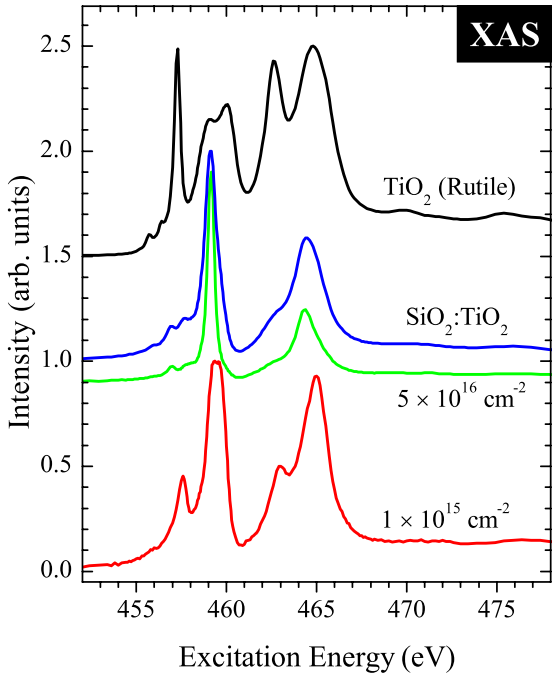

FIG. 2. Titanium $L_{2,3}$-edge X-ray absorption spectra for implanted and reference samples. The spectra have been offset vertically for clarity.

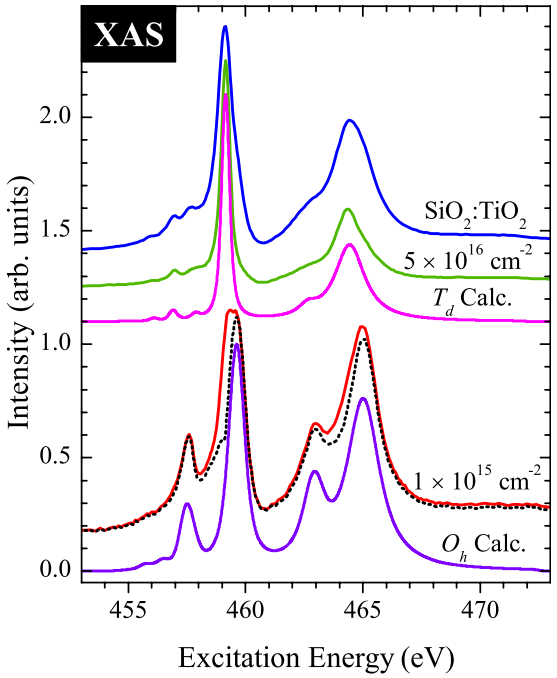

FIG. 3. Titanium $L_{2,3}$-edge X-ray absorption spectra for implanted and reference samples, along with calculated spectra of Ti^{4+} in T_d and O_h symmetries. The spectra have been offset vertically for clarity. The dotted spectrum is the result of subtracting 50% of the normalized 5×10^{16} cm^{-2} spectrum from the normalized 1×10^{15} cm^{-2} spectrum.

(and interfering) regions which are split apart by the $2p$ spin orbit coupling: the L_3 region below ~461 eV and the L_2 region above this point. Within each of these regions, peaks are split apart generally by local crystal field effects. For TiO_2, for example, the L_2 and L_3 regions are split into roughly two peaks each, which correspond approximately to the e_g levels (at higher energies) and t_{2g} levels (at lower energies), due to the O_h coordination of the Ti ions. Note that there are other minor peaks present due to multiplet effects and that the e_g peaks exhibit a small splitting due partially to symmetry distortion and partially due to long-range effects.[23,26]

Since the multiplet structures of these systems are well-described by MCFT, simulations were performed to determine the origin of the differences between the samples. The simulation results are shown in Figure 3, along with the corresponding experimental spectra. First considering the higher fluence case, we see excellent agreement is obtained with a calculation of a Ti^{4+} ion in tetrahedral (T_d) symmetry, using a 10 Dq value of −0.90 eV. This 10 Dq value is the energy splitting of the e and t_2 orbitals induced by bonding with neighboring atoms that distort the Ti $3d$ atomic orbitals from spherical symmetry. The negative sign indicates a tetrahedral T_d rather than octahedral O_h symmetry. This tetrahedral coordination of the Ti ions indicates they have been incorporated into Si sites of the SiO_2, and the spectra show a similar shape to experimental spectra of T_d Ti^{4+} in Ba_2TiO_4.[27] For the lower fluence case, however, the spectrum is best fit with a field of O_h symmetry (all parameters are shown in Table I). Here, a splitting of 1.75 eV was used, which is similar in magnitude compared to splittings found for other Ti^{4+} O_h systems such as $FeTiO_3$.[28] However, an additional Gaussian-like broadening is present in the experimental spectrum. To best reproduce the experimental data, an additional value of 0.25 eV was added to the FWHM of the Gaussian convolved with the simulated spectrum, compared to that of the T_d simulation (the same Lorentzian lifetime broadening was applied in each case). This additional broadening suggests that in this case the Ti ions are possibly located in interstitial regions of the SiO_2, where varying crystal field effects at different sites with varying geometries would broaden the spectrum. Finally, we note that the evident splitting of the peak at 459.4 eV for the 1×10^{15} cm^{-2} sample indicates there are some T_d–coordinated Ti ions in this sample as well. A subtraction of a 50% fraction of the normalized higher fluence spectrum from the normalized lower fluence spectrum yields the dotted curve overlaid with the lower fluence spectrum. While this analysis is not meant to be quantitative, it does remove the lower half of the most intense peak and improves the agreement with the calculation, strongly suggesting that there are some T_d coordinated Ti ions present in the lower fluence sample.

Figure 4 displays the oxygen K-edge XAS and XES for the reference a-SiO_2 and the Ti-containing samples. Using these spectra, one can investigate the oxygen $2p$–projected conduction and valence bands, respectively. Focusing on the XES first, we see minimal changes in the shape of the spectra for the various samples shown. As clarified in the inset, the spectra only gradually gain a small amount of spectral weight

TABLE I. Parameters used for the multiplet crystal field theory calculations. κ are rescaling factors for the intra-atomic Slater integrals, given as fractions of the Hartree Fock values.

Ion	Symmetry	10 Dq (eV)	κ
Ti^{4+}	O_h	1.75	0.75
Ti^{4+}	T_d	−0.90	0.65

on the low energy side of the main peak as the Ti content is increased. More significant changes are evident in the XAS, however, as prominent features are introduced in the pre-edge region from 531–535 eV as Ti is added to the samples. Stronger changes in the XAS compared to XES are expected, as the formally empty 3*d* shell of the Ti^{4+} ions means there are no occupied *d* states to contribute to the XES whereas there are ample empty states to contribute to the XAS.

The conduction band minimum (CB_{min}) and valence band maximum (VB_{max}) can be extracted from the XAS and XES using the second derivative technique,[29] and from these values the electronic band gap can be estimated. The second derivatives of the SiO_2 and SiO_2:TiO_2 spectra are shown at the bottom of Figure 4. It is found that both samples share a common VB_{max}, marked at point *a*, whereas the SiO_2:TiO_2 has a much lower conduction band minimum (point *b*) than pure SiO_2 (point *c*). Computing the differences between the maxima and minima yields estimated band gaps of 8.0 ± 0.3 eV for SiO_2 and 4.1 ± 0.3 eV for SiO_2:TiO_2. Within experimental error, the 5×10^{16} cm^{-2} sample has the same CB_{min} and VB_{max} as SiO_2:TiO_2 but is not shown for clarity. These results agree with an earlier optical study which found a gap of 4 eV for SiO_2:Ti synthesized using flame hydrolysis.[7] However, here we can show that this reduction from the pure SiO_2 gap is due entirely to changes in the conduction band minimum energy.

IV. DISCUSSION

The Ti *L* edge results show very different relative amounts of T_d Ti coordination for the two samples. Two possible explanations for this can be considered. First, the T_d coordination may be part of a stable phase of material where a certain ratio of Si and Ti is present. When too little Ti is present, it might not be energetically favorable to form Ti–O tetrahedra, and the Ti remains as interstitials. A second explanation is that with higher fluence, more damage to the host SiO_2 occurs during implantation. The higher degree of damage might allow for more incorporation of Ti into T_d sites. A preference to either explanation does not seem evident from the present results, but future experiments could be tailored to study this. Moreover, the specific changes induced by annealing could also be studied in future work since previous studies have found clusters of amorphous silicides[13] and highly conductive metallic Ti layers[15] in non-annealed samples synthesized with only slightly higher fluences than those used here. The application of *L*-edge XAS would provide a very useful study of the effects of the annealing process.

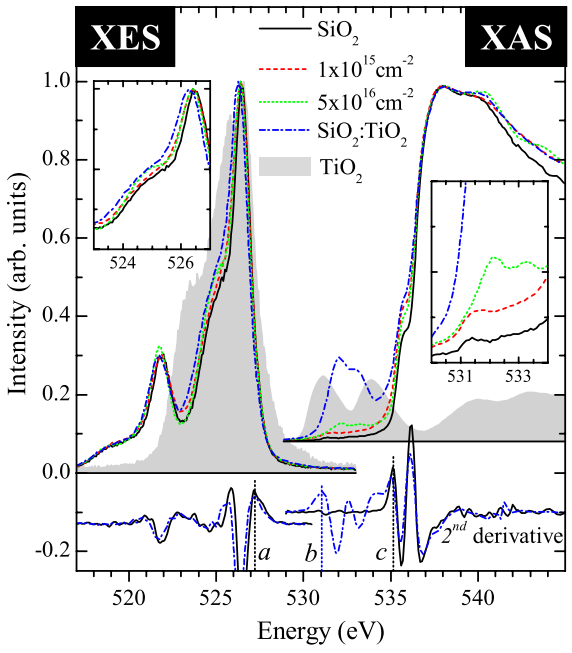

FIG. 4. Oxygen *K*-edge X-ray absorption (right) and emission (left) spectra for implanted and reference samples. The XAS spectra have been offset vertically for clarity. For two of the samples, the second derivatives of the spectra are shown below and the common valence band maximum energy *a* and the conduction band minimum energies (*b* for SiO_2:TiO_2, *c* for SiO_2) are marked with vertical dotted lines.

The oxygen edge results show the Ti induces a large effect on the SiO_2 band gap, reducing it to a range that is almost useful for electronic applications. The edge onset region of the O *K* XAS is generally very sensitive to transition metal 3*d* and oxygen 2*p* hybridization whereas the higher energy features are more sensitive to *sp* hybridization.[30] The 3*d*-sensitive region near the edge is often split into two peaks, and the degree of splitting is related to the local crystal field splitting. For TiO_2 this splitting is very prominent, as shown in the XAS spectrum in Figure 4 (in the region from 530 to 535 eV). For the SiO_2:TiO_2 and 5×10^{16} cm^{-2} samples, however, this splitting is reduced, in agreement with the weaker T_d crystal field splitting found from the Ti *L*-edge XAS analysis. As clarified in the right hand inset of Figure 4, the lower fluence sample yields a spectrum very similar to the pure SiO_2 reference—both show a small bump at ~531.5 eV (likely due to defect states in the SiO_2), the two-peaked Ti structure is not evident, and there is only a somewhat constant increase in spectral weight for the lower fluence spectrum compared to SiO_2. The similarity of these spectra is perhaps not surprising, for a few reasons. First, there are ~50 times fewer Ti atoms in the 1×10^{15} cm^{-2} sample compared to the 5×10^{16} cm^{-2} sample so the Ti 3*d* character is expected to be very weak. Second, if the Ti atoms in the lower fluence sample are located primarily in interstitial regions as suggested earlier, the covalent interaction between the Ti and O atoms will be reduced, compared to the case where they are located in well defined tetrahedra. Third, the extra broadening that smeared the features of the Ti *L* edge XAS for the lower fluence sample would also affect the presence of the two-peaked structure in the O *K* XAS spectrum of this sample. Thus, the lack of distinct Ti 3*d* features in the 530–535 eV region is reasonable. Finally, we note that while the empty *d* shell for Ti leads to strong conduction band changes, the fuller *d* shells for elements like Ni and Cu should lead to useful changes in the valence band properties. By combining Ti implantation with Ni or Cu, one could then tailor both the valence and conduction bands, enabling further control over the band gap.

V. CONCLUSIONS

To conclude, we have studied Ti ion implanted SiO_2 samples and reference materials using soft XAS and XES.

The sensitivity of the Ti $L_{2,3}$ XAS to the Ti coordination was demonstrated, and it was shown that octahedral Ti coordination (possibly in interstitial regions) can be obtained by lowering the implantation fluence, while for high fluence the Ti showed tetrahedral coordination. Oxygen *K*-edge XAS spectra were used to probe the hybridization of the Ti 3*d* and O 2*p* states in the conduction band. Strong hybridization was observed for the high fluence and reference samples whereas the low fluence sample showed minimal interaction. From the oxygen XAS and XES the band gaps were extracted, yielding 8.0 ± 0.3 eV for SiO_2 and 4.1 ± 0.3 eV for a sample implanted with 5×10^{16} cm^{-2} ions (and for a SiO_2:TiO_2 reference sample). These results demonstrate a change in Ti coordination with a change in fluence and the same post-implantation annealing, reveal the mechanism behind band gap reduction in SiO_2:Ti materials, and show the applicability of *L*-edge XAS with a multiplet crystal field theory interpretation for studying Ti coordination in novel materials.

ACKNOWLEDGMENTS

The present study was carried out under the support of the Natural Sciences and Engineering Research Council of Canada (NSERC), the Canada Research Chair program, the Ural Division of the Russian Academy of Sciences (Project No. 12-I-2-2040), and the Russian Science Foundation for Basic Research (Project No. 11-02-00022). Assistance from the staffs of the Advanced Light Source and Canadian Light Source is gratefully acknowledged. The Advanced Light Source is supported by the Director, Office of Science, Office of Basic Energy Sciences, of the U. S. Department of Energy under Contract No. DE-AC02-05CH11231. The Canadian Light Source is supported by NSERC, the National Research Council (NSC) Canada, the Canadian Institute of Health Research (CIHR), the Province of Saskatchewan, Western Economic Diversification Canada, and the University of Saskatchewan.

[1]S. B. Ogale, Adv. Mater. **22**, 3125 (2010).
[2]S. A. Wolf, D. D. Awschalom, R. A. Buhrman, J. M. Daughton, S. von Molnar, M. L. Roukes, A. Y. Chtchelkanova, and D. M. Treger, Science **294**, 1488 (2001).
[3]H. Hosono, Jpn. J. Appl. Phys. **32**, 3892 (1993).
[4]E. Cattaruzza, Nucl. Instrum. Methods Phys. Res., Sect. B **169**, 141 (2000).
[5]A. Meldrum, R. F. Haglund, L. A. Boatner, and C. W. White, Adv. Mater. **13**, 1431 (2001).
[6]A. L. Stepanov, Rev. Adv. Mater. Sci. **27**, 115 (2011).
[7]S. C. Cheng, J. Non-Cryst. Solids **354**, 3735 (2008).
[8]G. S. Henderson, X. Y. Liu, and M. E. Fleet, Mineral. Mag. **67**, 597 (2003).
[9]G. S. Henderson, X. Liu, and M. E. Fleet, Phys. Chem. Minerals **29**, 32 (2002).
[10]C. F. Song, M. K. Lu, P. Yang, D. Xu, and D. R. Yuan, J. Sol-Gel Sci. Technol. **25**, 113 (2002).
[11]M. W. Gaultois and A. P. Grosvenor, J. Mater. Chem. **21**, 1829 (2011).
[12]V. F. Lebedev, V. V. Koltashev, E. B. Kryukova, V. G. Plotnichenko, and A. O. Rybaltovsky, Phys. Chem. Glasses **43C**, 141 (2002), http://www.ipme.ru/e-journals/RAMS/no_22711/stepanov.html.
[13]E. Cattaruzza, G. Mattei, P. Mazzoldi, R. Bertoncello, G. Battaglin, and L. Mirenghi, Appl. Phys. Lett. **67**, 2884 (1995).
[14]V. Belostotsky, J. Non-Cryst. Solids **202**, 194 (1996).
[15]P. Martin, M. Dufour, A. Ermolieff, S. Marthon, F. Pierre, and M. Dupuy, J. Appl. Phys. **72**, 2907 (1992).
[16]Z. Pan, S. H. Morgan, D. O. Henderson, R. H. Magruder III, and R. A. Zuhr, Nucl. Instrum. Methods Phys. Res. B **114**, 281 (1996).
[17]J. P. Zhao, Z. Y. Chen, M. Lu, and J. W. Rabalais, J. Appl. Phys. **93**, 566 (2003).
[18]V. S. Kortov, D. A. Zatsepin, A. F. Zatsepin, N. V. Gavrilov, and E. Z. Kurmaev, Russian Federation patent no. RU 2461665 C1 (2012).
[19]J. F. Ziegler, J. P. Biersack, and M. D. Ziegler, *SRIM - The Stopping and Range of Ions in Matter* (SRIM Co., 2008).
[20]J. J. Jia, T. A. Callcott, J. Yurkas, A. W. Ellis, F. J. Himpsel, M. G. Samant, J. Stöhr, D. L. Ederer, J. A. Carlisle, E. A. Hudson, L. J. Terminello, D. K. Shuh, and R. C. C. Perera, Rev. Sci. Instrum. **66**, 1394 (1995).
[21]T. Regier, J. Krochak, T. K. Sham, Y. F. Hu, J. Thompson, and R. I. R. Blyth, Nucl. Instrum. Methods Phys. Res. A **582**, 93 (2007).
[22]F. M. F. de Groot, M. A. Arrio, P. Sainctavit, C. Cartier, and C. T. Chen, Solid State Commun. **92**, 991 (1994).
[23]F. de Groot and A. Kotani, *Core Level Spectroscopy of Solids*, Advances in Condensed Matter Science Series (CRC, 2008).
[24]F. M. F. Groot, M. O. Figueiredo, M. J. Basto, M. Abbate, H. Petersen, and J. C. Fuggle, Phys. Chem. Miner. **19**, 140 (1992).
[25]S. Shin, M. Fujisawa, H. Ishii, Y. Harada, M. Watanabe, M. M. Grush, T. A. Callcott, R. C. C. Perera, E. Z. Kurmaev, A. Moewes, R. Winarski, S. Stadler, and D. Ederer, J. Electron Spectrosc. Relat. Phenom. **92**, 197 (1998).
[26]P. Krüger, Phys. Rev. B **81**, 125121 (2010).
[27]R. Brydson, L. A. J. Garvie, A. J. Craven, H. Sauer, F. Hofer, and G. Cressey, J. Phys.: Condens. Matter **5**, 9379 (1993).
[28]F. M. F. de Groot, J. C. Fuggle, B. T. Thole, and G. A. Sawatzky, Phys. Rev. B **41**, 928 (1990).
[29]E. Z. Kurmaev, R. G. Wilks, A. Moewes, L. D. Finkelstein, S. N. Shamin, and J. Kuneš, Phys. Rev. B **77**, 165127 (2008).
[30]F. M. F. de Groot, M. Grioni, J. C. Fuggle, J. Ghijsen, G. A. Sawatzky, and H. Petersen, Phys. Rev. B **40**, 5715 (1989).